Environmental Science & Technology

pubs.acs.org/est

Article

New Insights into Aggregation Behaviors of the UV-Irradiated Dissolved Biochars (DBioCs) in Aqueous Environments: Effects of Water Chemistries and Variation in the Hamaker Constant

Ning Tang, Yihui Guo, Ziqian Zhu, Longbo Jiang, Na Li, Tingting Hu, Lan Lu, Jingyi Zhang, Xiaodong Li, and Jie Liang*

Cite This: *Environ. Sci. Technol.* 2024, 58, 8053−8064

Read Online

ACCESS | Metrics & More | Article Recommendations | Supporting Information

ABSTRACT: The aggregation behavior of ubiquitous dissolved black carbon (DBC) largely affects the fate and transport of its own contaminants and the attached contaminants. However, the photoaging processes and resulting effects on its colloidal stability remain yet unknown. Herein, dissolved biochars (DBioCs) were extracted from common wheat straw biochar as a proxy for an anthropogenic DBC. The influences of UV radiation on their aggregation kinetics were systematically investigated under various water chemistries (pH, electrolytes, and protein). The environmental stability of the DBioCs before and after radiation was further verified in two natural water samples. Hamaker constants of pristine and photoaged DBioCs were derived according to Derjaguin−Landau−Verwey−Overbeek (DLVO) prediction, and its attenuation ($3.19 \pm 0.15 \times 10^{-21}$ J to $1.55 \pm 0.07 \times 10^{-21}$ J after 7 days of radiation) was described with decay kinetic models. Pearson correlation analysis revealed that the surface properties and aggregation behaviors of DBioCs were significantly correlated with radiation time ($p < 0.05$), indicating its profound effects. Based on characterization and experimental results, we proposed a three-stage mechanism (contended by photodecarboxylation, photo-oxidation, and mineral exposure) that DBioCs might experience under UV radiation. These findings would provide an important reference for potential phototransformation processes and relevant behavioral changes that DBC may encounter.

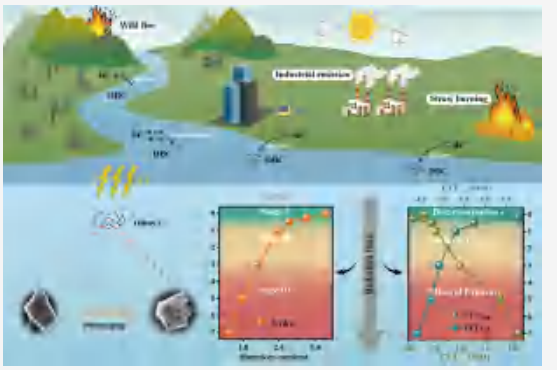

KEYWORDS: *dissolved biochars (DBioCs), aggregation kinetics, Hamaker constant, UV radiation, photoaging*

1. INTRODUCTION

Black carbon (BC), a collective term for organic residue produced during incomplete combustion of biomass or fossil fuels, exists widely in the natural environment.[1,2] Its global annual production is as much as 50−270 Tg C (1 Tg = 10^{12} g), 80% of which is entrapped in soil.[3,4] The dissolved fraction (DBC, <0.45 μm) eventually enters the aqueous media via runoff and infiltration.[5,6] With the high affinity and strong colloidal stability,[7,8] DBC may carry various environmental contaminants over long-distance once in the water,[9−11] playing vital roles in carbon cycling, climate change, and human health.[12−14] However, the research on aggregation of DBC that largely dominates the carbon flux is far from sufficient,[15] in contrast with more concerns on that of carbonaceous nanoparticles (e.g., graphene oxide (GO),[16,17] carbon nanotubes (CNTs),[18] fullerenes (C_{60}),[19−21] etc.), metal-(oxide),[22−25] and nanoplastics.[26,27] Indeed, DBC has much higher environmental relevant concentration and suspending capability than these engineered nanomaterials[28] and is more worthy of attention.

Upon being released into the environment, BC will inevitably undergo aging, involving physical,[29,30] chemical,[31] and biological processes.[32] Photoaging is particularly important for DBC in sunlit waters. As one of the most photosensitive components in natural organic matters (NOM),[33] it can be excited by photons to produce ^{3}DBC* and various reactive oxygen species (ROS).[34,35] These active species can significantly change the physicochemical properties of DBC,[36] via various mechanisms, commonly including photo-oxidation,[37] photodecarboxylation,[38] and photobleaching.[39] Thus, the photoaging could be another crucial factor affecting DBC colloidal stability besides water chemistries, e.g., pH, electrolytes, and NOM.[40] But opinions on its influence are widely varying. Xu et al. found that sunlight exposure led to enhanced

Received: January 22, 2024
Revised: April 8, 2024
Accepted: April 9, 2024
Published: April 25, 2024

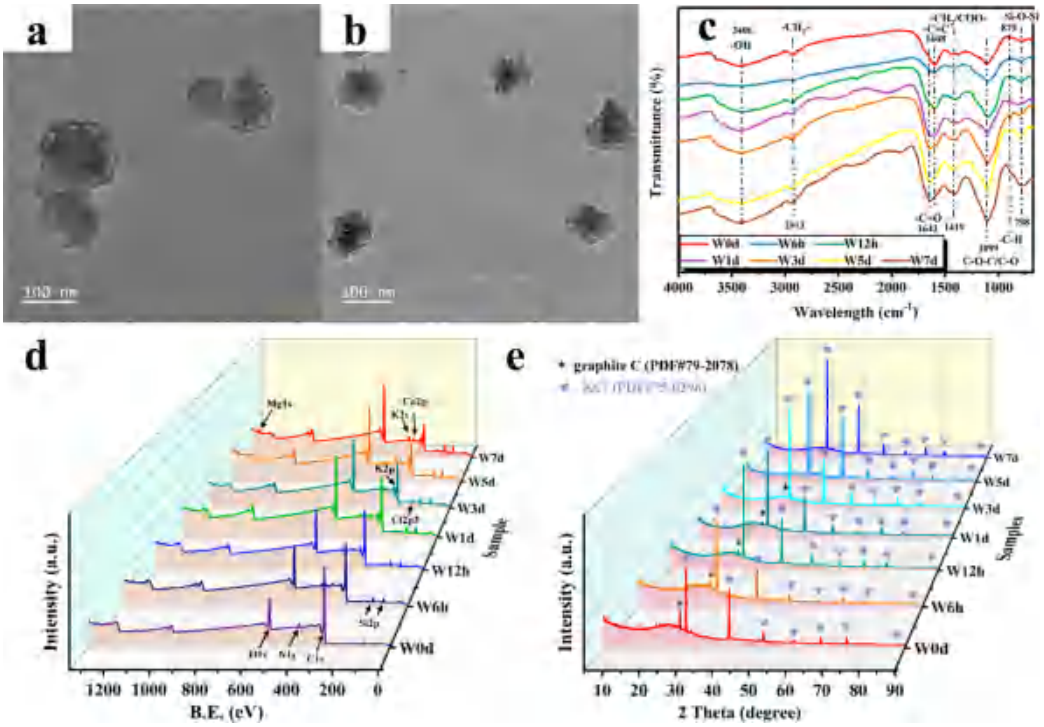

Figure 1. Characteristics of DBioCs. TEM images of (a) W0d and (b) W7d, (c) FT-IR spectra, (d) X-ray photoelectron spectroscopy (XPS) analyses, and (e) XRD spectra for pristine and photoaged DBioCs. It can be seen from TEM images that the biochar particles were evenly dispersed in the suspension. After irradiation, the particles got a more irregular shape, rougher surface, and smaller size, which is consistent with the results of SEM images (Figure S4). FT-IR spectra revealed the changes of surface functional groups of DBioCs. As aging proceeds, the surface oxygen-containing function groups (−OH, −C═O, C−O−C/C−O, etc.) increased significantly, except for W6h. XPS and XRD data recorded the gradual processes of DBioCs with the strengthened O 1s peak, the weakened C 1s peak, the disappeared graphite C, and the exposited mineral elements under the UV irradiation.

colloidal stability of DBC extracted from bamboo-shavings biochar.[15] However, lower critical coagulation concentrations (CCCs) occurred on dissolved black nitrogen (DBN) and DBC extracted from wood-shavings biochar in an NaCl solutions after xenon-lamp radiation.[41] These photoinduced variations in DBC stability were explained by surface potentials and reactivity, but its possible impacts on intrinsic attributes of materials, e.g., Hamaker constant, were often overlooked. This constant is a key parameter for assessing van der Waals (vdW) attraction.[42] Its value, immune to environmental conditions, is only related to materials' inherent structure.[43] As reported, sunlight can degrade the chromophores and even mineralize DBC.[36,37] Such a drastic evolution inspired us that photoaging may change the DBC structure, thus affecting its Hamaker constant, which has recently been confirmed in soot nanoparticles (SNPs).[44] However, there have been, hitherto, few studies on the Hamaker constants of DBC, let alone the impact of the aging processes on them. Therefore, exploring the photoaging mechanism, establishing the relation between photoaging and colloidal stability, and determining the variation rules on the Hamaker constant under photoaging are imperative to accurately describe and predict the actual environmental behaviors of DBC.

Herein, dissolved biochars (DBioCs) extracted from wheat straw biochar were used as proxies for DBC. Our objectives were to (1) investigate the aggregation behaviors of DBioCs under different water chemistries (pH, IS, and cation type); (2) quantify the changing trends in the Hamaker constant and photoaging process of DBioCs with radiation time; and (3) inspect the colloidal stabilities of pristine and photoaged DBioCs in the presence of bovine serum albumin (BSA) and natural water. Insights gained from these findings should be significant in predicting the environmental behavior and fate of DBC, especially those exposed to sunlight.

2. MATERIALS AND METHODS

2.1. Chemicals. NaCl, $CaCl_2$, BSA powder, and pH adjustors (i.e., NaOH and HCl) of analytical grade were purchased from Sinopharm Chemical Reagent Co., Ltd. (Shanghai, China). All water used was deionized (DI) water with resistivity > 18.25 MΩ·cm^{-1}.

2.2. Preparation of DBioCs. Biochar was produced under anaerobic conditions using a patented slow-pyrolysis process (China patent No. ZL200920232191.9).[9] The bulk biochar was first homogenized by ball-milling and then dispersed in DI water. The pristine DBioC (W0d) was obtained via a series of operations including ultrasound, deposition, filtration, and freeze-drying. The details are shown in TEXT S1, Supporting Information (SI).

2.3. Irradiation Experiments. The irradiation experiment was conducted in a BILON-GHX-V photochemical reactor (Bilon. China) equipped with a 1000 W Hg lamp (λ = 200−600 nm) (Figure S1). With the assistance of a photoradiometer (PL-MW 2000, Perfectlight, China), the light intensity provided by the lamp was measured to be nearly 100 mW·cm^{-2} on quartz sample tubes, which is equivalent to that of solar light in summer at the equator.[45] More details are shown in TEXT S2. The obtained DBioCs, assigned as W0d, W6h, W12h, W1d, W3d, W5d, and W7d, were stored in a desiccator for backup.

https://doi.org/10.1021/acs.est.4c00780
Environ. Sci. Technol. 2024, 58, 8053−8064

2.4. Characterizations. The pHs of DBioCs suspensions before and after radiation were recorded by a pH meter (PHS-3E, INESA, China), and their hydrodynamic sizes (D_h) and ζ potential distributions in DI water were measured using Zetasizer Nano ZS (Malvern, U.K.). The morphology of DBioCs was characterized using field-emission scanning electron microscopy (SEM, ZEISS Sigma 300, Germany) and transmission electron microscopy (TEM, FEI Tecnai F20, U.S.). X-ray diffraction (XRD) data were analyzed with the help of a diffractometer (Rigaku SmartLab SE, Japan). Surface properties of DBioCs were identified by X-ray photoelectron spectroscopy (XPS, Thermo Scientific K-Alpha, U.S.) and Fourier transform infrared spectroscopy (FT-IR, NICOLET iN10, Thermo Fisher Scientific, U.S.). The elemental compositions of bulk DBioCs were determined using an element analyzer (EA, Vario EL Cube, Elementar, Germany). Based on the EA and XPS data, the bulk and surficial O/C ratios were calculated. In order to eliminate the possible interference from dissolved small molecules and salts, DBioCs samples were ultrafiltered to conductivities of the filtrates less than 5 μS/cm using a molecular weight cutoff of 100 kDa (Millipore, U.S.) before FT-IR, XPS, and elemental analysis measurements. The detailed information was described in TEXT S4.

2.5. Aggregation Kinetics. Before the aggregation experiments, the freeze-dried DBioCs powder was accurately weighed (2.5 ± 0.1 mg) and mixed with about 30 mL of DI water. After 1 h of ultrasonic treatment, the mixtures were further treated by a cell crusher (KM-450D, Kunshan Meimei, China, 450 KW, 20 kHz, 10 s on, and 5 s off) for 1 h to ensure the complete dispersion, followed by another 1 h of ultrasound to stabilize the colloidal systems. Then the well-dispersed samples were added to DI water, yielding 50 mg-DBioCs/L stock suspensions, and immediately subjected to the aggregation experiments under the designed conditions (TEXT S5).

2.6. Natural Water Sampling. Two different natural water samples were collected from the Xiangjiang River (N 28°11′1″, E 112°56′55″) and Taozihu Lake (N 28°11′1″, E 112°56′51″) using precleaned polyethylene containers (Figure S2). Although close in distance, they are typically flowing and enclosed waters, respectively. After returning to the lab, both of them were filtered through a 0.45 μm membrane, characterized, and then stored at 4 °C.[46] The pH (7.34 ± 0.03 vs 7.75 ± 0.10), TOC (2.26 mg/L vs 3.65 mg/L), and electric conductivity (194.3 ± 0.5 μS/cm vs 391.6 ± 1.0 μS/cm) of the Xiangjiang sample were lower than those of the Taozihu one. They have the same most abundant univalent (Na^+) and divalent (Ca^{2+}) cations and anions (SO_4^{2-}) (Table S1). For the sake of testing the aggregation behavior of DBioCs in natural water, filtered water samples were employed to replace the DI water, and other operations were the same as the aggregation experiments (TEXT S5).

3. RESULTS AND DISCUSSION

3.1. Characterization of DBioCs before and after UV Radiation. All DBioCs formed dark-brown suspensions in DI water, and no obvious aggregation/sedimentation occurred within 30 days (Figure S3), suggesting their long-term stability. TEM images exhibited the irregular-shape of typical DBC (Figures 1a and 1b).[11] SEM images recorded the gradual roughening and fragmentation of DBioCs during aging (Figure S4), which might be caused by the attack of UV-induced ROS.[47] Figure S5 revealed size distributions of pristine and radiated DBioCs. The z-average D_h of fresh DBioCs (W0d) is 263.50 ± 5.70 nm with a polydispersity index (PDI) of 0.24 ± 0.04 (Figure S6), close to that of GO[16] and pinewood-chips-derived biochar colloids.[31] This value fluctuated with radiation gradually instead of decreasing as polystyrene nanoparticles (PSNPs) did.[43] Compared with nanoplastics, DBioCs have highly complex composition and structure.[48] The increased D_h values upon radiation ($r = 0.657$, $p = 0.109$) may result from the presence of a hydration layer.[49] Nevertheless, on the whole, the variation in D_h was not drastic over the experiment periods, and all PDI values were less than 0.3, indicating that UV-radiation did not change the good dispersibility of DBioCs.[50] The fluctuations also appeared in their zeta potentials ($r = 0.221$, $p = 0.634$), which ranged from −47.10 ± 1.12 mV (W3d) to −42.10 ± 0.61 mV (W7d), experiencing an increase (W0d → W6h), a decrease (W6h → W3d), and then an increase (W3d → W7d) (Figure S6b).

Figure 1c exhibited the typical FT-IR spectra of biochar with characteristic peaks of −OH (3406 cm^{-1}), aliphatic $-CH_2-$ (2913 cm^{-1}), −C═O (1643 cm^{-1}), aromatic C═C (1608 cm^{-1}), −COO− (1419 cm^{-1}), C−O−C/C−O (1099 cm^{-1}), and aromatic C−H (879 cm^{-1}).[31,51,52] With radiation, the −OH band and C−O−C/C−O peak became significantly wider and deeper, while the C═C peak tended to shift toward the −C═O one. It suggested that more oxygen-containing function groups (OFGs) appeared on the DBioCs surface,[53] which was confirmed by XPS spectra (Figure 1d). The peak area of C 1s decreased gradually, and that of O 1s increased remarkably. The surficial O/C ratio thus rose from 0.32 (W0d) to 0.98 (W7d) ($p < 0.001$), indicative of the higher surface polarity of DBioCs as photoaging.[51] This was in line with the polarity indexes (O/C and (O+N)/C ratios) obtained by EA data (Table S2). Although there was a slight difference in values between surficial and bulk O/C ratios, their trends with radiation time were highly consistent ($p < 0.001$) (Figure S7). The bulk O/C and (O+N)/C ratios increased from 0.26 and 0.30 (W0d) to 0.60 and 0.64 (W7d), getting closer to the average values of environmental humic substances (0.58 ± 0.08 for O/C and 0.62 ± 0.08 for (O+N)/C) provided by the International Humic Substances Society (IHSS).[14] It implied that UV radiation might promote the evolution of DBioCs toward humic substances. Moreover, the H/C ratio rose from 0.06 (W0d) to 0.07 (W7d) ($p = 0.01$), indicating the declined aromatization degree of DBioCs.[54] Reflecting in the XRD pattern (Figure 1e), the symmetric peak at ∼26.6° diminished and eventually disappeared after 5 days of radiation, demonstrating that graphite C transited to an amorphous state gradually.[10] The enhanced KCl peak (PDF #75−0296) after photoaging implied that the UV-radiation could expose minerals on the DBioCs surface. This was in conformity with the enhancement of the Si−O−Si peak (798 cm^{-1}) in the FT-IR spectra (Figure 1c), the peak's appearance of Mg 1s, Ca 2p, K 2p, and Cl 2s in the XPS spectra (Figure 1d), and the increased ash content obtained by EA data (Table S2).[55]

3.2. Aggregation Kinetics of DBioCs at Various Solution pHs. The influence of pH on pristine DBioC was tested in NaCl solutions (10−1000 mM) at pH 5, 7, and 9, respectively. These conditions encompassed the typical IS and pH values in surface waters.[56] As shown in Figure S8, all DBioCs had zeta potentials less than −30 mV over the tested pH range, suggesting their electrostatic stability.[57] However, these values gradually increased with increasing electrolyte

https://doi.org/10.1021/acs.est.4c00780
Environ. Sci. Technol. 2024, 58, 8053−8064

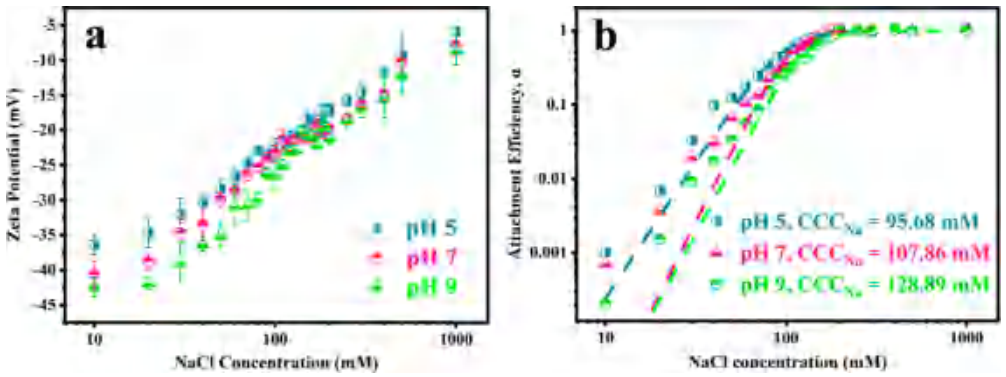

Figure 2. Aggregations of pristine DBioCs in an NaCl solutions with various pHs (5, 7, and 9). (a) The variations in zeta potentials of DBioCs, as a function of NaCl concentration (10−1000 mM), and (b) aggregation attachment efficiencies (α) of DBioCs at pH 5, 7, and 9 (data points, experimentally measured based on eq S2, and dotted lines, theoretically fitted by eq S3, and critical coagulation concentration (CCC) values were yielded on the basis of eq S3 with $R^2 > 0.98$). All experiments were carried out at 12.5 mg-DBioCs/L and 25 °C.

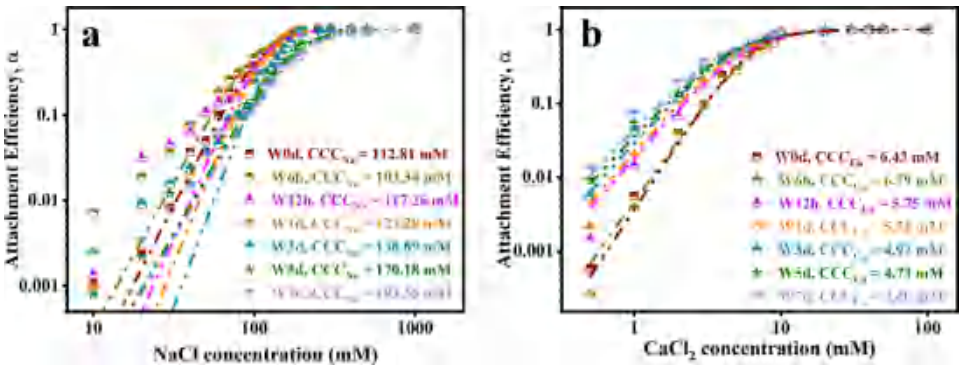

Figure 3. Colloidal stability of DBioCs before and after UV irradiation. Attachment efficiencies (α) of DBioCs as a function of (a) NaCl (10−1000 mM) and (b) $CaCl_2$ concentration (0.5−100 mM) after 0 d, 6 h, 12 h, 1 d, 3 d, 5 d, and 7 d of UV radiation (data points, experimentally measured based on eq S2, and dotted lines, theoretically fitted by eq S3, and critical coagulation concentration (CCC) values were yield on the basis of eq S3 with $R^2 > 0.98$). All experiments were carried out at 12.5 mg-DBioCs/L and 25 °C.

concentrations (Figure 2a). Correspondingly, the colloidal stability was challenged. The aggregation profiles of W0d as a function of NaCl concentration conformed to classical DLVO-type interaction with distinct reaction-limited (RLCA) and diffusion-limited (DLCA) regimes (Figure S9a-c).[57] The CCC_{Na} values calculated according to eq S3 were 95.68 mM, 107.86 mM, and 128.89 mM at pH 5, 7, and 9, respectively (Figure 2b). Obviously, acidic conditions were more favorable for DBioCs aggregation, whereas the opposite was true for the alkaline counterpart. This phenomenon also appeared in particles reported elsewhere.[58,59] The reason may be manifold. For one thing, under acidic conditions, excess free H^+ served as a counterion compressing the electric double layer (EDL) and protonated the DBioCs surface groups (e.g., −OH and −COOH), which made the DBioCs surface less negatively charged (Figures 2a and S8). For another, more H-bond formed between W0d and water at a higher pH may wrap the DBioCs surface with a layer of water sheath,[60] which is not conducive to the mutual collision and adhesion of particles. Apart from CCC_{Na} values, the pH-dependent characteristic also was reflected in the fast aggregation rate (k_{fast}). As exhibited in Figure S9d, the k_{fast} value gradually decreased from 1.05 (pH 5) to 0.75 (pH 7) and 0.69 nm/s (pH 9) (p = 0.121), indicating that protons promote faster aggregation for W0d in the initial stage. The aggregations of other DBioCs at different pHs also showed similar patterns (Figure S10). After exploring TEXT S6, we believe that the lower aggregation rate under higher pH was caused by enhanced hydrogen bonding of DBioCs, which increased the solution viscosity. Moreover, the pH dependence of k_{fast} may be affected by the nature of the interested particles. For example, Wang et al. reported the k_{fast} values of engineered nanoparticles and kaolin clays were nonmonotonic functions of pH.[22] So far, it remains unclear how the particle properties affect the pH dependence of k_{fast}.

These findings imply that DBioCs drifting in natural waters may undergo significant changes in their colloidal stability when encountering pH-abrupt regions (e.g., acidic wastewater outfalls) or unexpected events (e.g., acid rain) even in the environmentally relevant pH (5−9). It might profoundly affect the environmental fate of DBioCs themselves and adsorbed pollutants. Therefore, the transient variations in DBioCs aggregation behavior under these changing events are worthy of further investigation.

3.3. Effects of Irradiation Time on the Colloidal Stability of DBioCs. In the electrolyte-free systems, no significant aggregations were observed for all DBioCs (Figures S11a and S12a), implying their stability during the experiment period, regardless of irradiation. This may be attributed to the strong electrostatic repulsion, as evidenced by their highly negative charges (Figure S6b). However, their stability was disrupted in electrolyte solutions (Figures S11 and S12). Their zeta potentials were less negative with the electrolyte concentration (Figure S13). For instance, the ζ values of W0d shifted from −42.25 ± 1.01 mV at 10 mM NaCl to −8.52

https://doi.org/10.1021/acs.est.4c00780
Environ. Sci. Technol. 2024, 58, 8053−8064

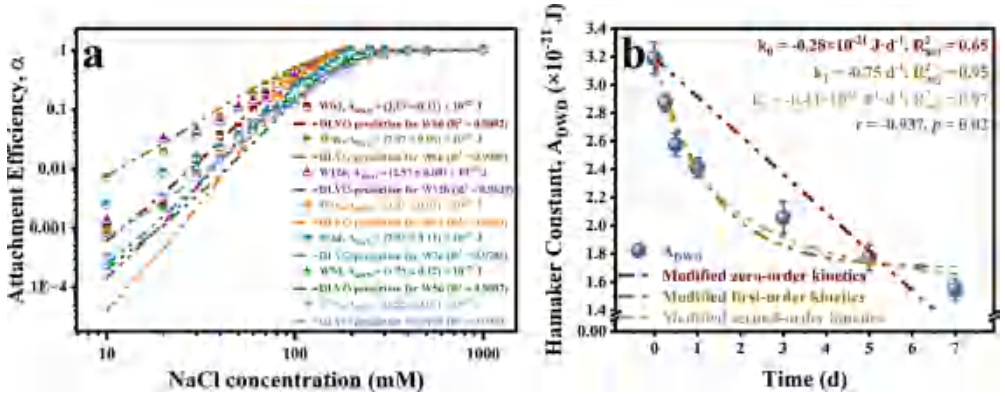

Figure 4. Predication and fitting for Hamaker constants of DBioCs. (a) Theoretical DLVO simulation (dotted lines, derived by eq S14) for experimentally obtained attachment efficiencies (data points, given by eq S3) of pristine and photoaged DBioCs in the NaCl solutions at unadjusted pH (~7.5). The yielded Hamaker constants (A_{DWD}) according to eq S14 for DBioCs were decreased from 3.19 ± 0.11 to 1.55 ± 0.07 × 10^{-21} J with UV exposure. (b) The nonlinear fitting of kinetic models (Modified zero-order, first-order, and second-order models) for A_{DWD} of DBioCs decaying with UV radiation duration.

± 2.91 mV at 1000 mM NaCl. It means the substantially weakened electrostatic repulsion between DBioCs at high counterion concentrations.[61] In comparison to Na^+, Ca^{2+} has a remarkably stronger ability to shield surface charges of DBioCs (Figure S13). Taking W0d as an example, 10 mM NaCl can only increase its zeta potential from −43.53 ± 0.51 mV to −42.23 ± 1.01 mV, while 10 mM $CaCl_2$ can make it to −12.80 ± 0.10 mV; 0.5 mM $CaCl_2$ can raise its zeta potential to −22.87 ± 0.50 mV, but more NaCl concentrations (>100 mM) were required to reach this value.

Aggregation profiles of DBioCs over time as a function of electrolyte concentrations are shown in Figures S11b-h and S12b-h. Figure 3 presented that all the stability profiles can be well quantified by eq S3 (R^2_{adj} > 0.98). For W0d, the obtained CCC_{Na} was 112.80 mM. It approached that for some carbonaceous particles like N-PBC500 (108 mM)[10] and WDBC700 (127 mM)[40] but was higher than that for nano activated carbons (NACs, 42.4−76.2 mM)[62] and various engineering nanomaterials (ENMs) involving CeO_2 (15 mM),[25] CuO (27.8 mM),[24] TiO_2 (50 mM),[22] and Ag NPs (12 mM).[23] It showed that W0d had colloidal stability higher than those of these widely concerned ENMs. The CCC_{Na} increased (p = 0.001) and k_{fast} values decreased (p = 0.002) with radiation, except W6h (Figures 3a and S11i), which means that UV-radiation may promote DBioCs dispersion and migration. This photoinhibited aggregation in NaCl solutions also occurred in nC_{60}[19] and PSNPs,[26] but the opposite was observed in DBN,[41] SNPs,[44] COOH-MWCNT,[18] GO NPs[17] and aged TiO_2.[63] This implies that the change in aggregation behaviors dominated by the aging process may vary from material to material.

Compared with aggregations in NaCl solutions, the behaviors of DBioCs in $CaCl_2$ were distinctly different (Figure 3b). Although the magnitude of changes in CCC_{Ca} and CCC_{Na} of DBioCs before and after radiation was similar (177.61% vs 154.22%), the former (4.40−6.43 mM) was significantly smaller than the latter (103.34−183.55 mM). These CCC_{Ca} approached those for black phosphorus (2.5 mM),[64] pristine and aged nC_{60} (3.24−4.25 mM),[19] fresh SNPs (3.5 mM),[44] and nano-BCs (2.7−4.3 mM)[51] but were less than those for WB300 (61.4 mM)[65] and pristine and aged PB300 and PB600 (25.2−58.6 mM).[31] The smaller CCC_{Ca} implies that DBioCs may tend to aggregate easier than WB300 and PB300 in a $CaCl_2$ solutions. The variation trends of CCC_{Ca} (p = 0.011) and k_{fast} (p = 0.003) with aging were opposite those in the NaCl solutions. It is consistent with the findings on PSNPs[43] and nC_{60},[19] despite there being also many publications revealing the photoinduced accordant tendency between them.[17,44,63] These discrepancies may result from differences in particle attributes and aging conditions. Larger k_{fast} and lower CCC appeared in the $CaCl_2$ solution (Figures S12i and Figure 3b), indicating that Ca^{2+} had a stronger capacity to destabilize DBioCs. According to the Schulze-Hardy rule, CCC is proportional to z^n (n = −6 to −2; z is ion valence).[58,66] Counterions with higher valence possess more efficient charge screening capability,[67] which echoes the above discussion on zeta potentials. CCC_{Ca}/CCC_{Na} ratios were $2^{-4.13}$, $2^{-3.92}$, $2^{-4.35}$, $2^{-4.51}$, $2^{-4.82}$, $2^{-5.17}$, and $2^{-5.38}$ for W0d, W6h, W12h, W1d, W3d, W5d, and W7d, respectively (Table S5), well obeying the Schulze-Hardy rule (TEXT S7). It once again verified that the aggregations of DBioCs may originate from EDL compression and charge screening.[67] Furthermore, the power term, n, gradually reduced as DBioCs aged (p = 0.001), consistent with previous research by Qu et al., wherein they found that 7 days of UV radiation decreased the n-value of nC_{60} from −4.3 to −7.1.[19] The Schulze-Hardy rule was proposed based on classical DLVO interactions, but some specific interactions, e.g., Ca^{2+} bridging, were not taken into account.[18,68] It may be the main reason why the n-value of DBioCs gradually decreased with radiation.[64] Reports on Ca^{2+} bridging-enhanced aggregation are readily available.[17] Herein, UV-increased OFGs provided more Ca^{2+} binding sites, resulting in a stronger bridging effect and a more significant aggregation enhancement.

Overall, DBioCs aggregations in water were mainly governed by the surface charge that was deeply affected by the ionic strength. This means that DBioCs well-suspended in freshwater may be destabilized and even separated out from the water column in some unexpected events (e.g., discharge of highly concentrated ionic water, etc.) or specific areas (e.g., estuaries, etc.). Sunlight exposure may alter the DBioCs surface chemistry, which resulted in higher stability in the presence of Na^+ (dominated by electrostatic repulsion) and easier aggregation in the presence of Ca^{2+} (dominated by bridging effect). This complex electrolyte association profoundly affects the possible behaviors of DBioCs in natural water.

https://doi.org/10.1021/acs.est.4c00780
Environ. Sci. Technol. 2024, 58, 8053−8064

3.4. Hamaker Constants of DBioCs Derived from the DLVO Theory. Na^+ is generally considered as a nonreactive ion,[15] and aggregation behaviors of particles in the presence of Na^+ can be roughly inferred by analyzing the surface charge. However, in this work, the variation in zeta potentials of DBioCs alone could not account for their increased CCC_{Na} values ($r = 0.187$, $p = 0.688$), especially for ones that suffered from long-time irradiation (W5d and W7d had less negative charges but higher CCC_{Na} values than did W3d did). It enlightens us that UV exposure may have other effects on DBioCs. According to the classical DLVO theory, we found that the parameter dominating the colloidal stability of particles was the Hamaker constant in addition to the surface potential. This crucial constant is considered to be an intrinsic property of the constituent materials[69] and should be a fixed value.[70] However, the surface dependence of the Hamaker constant has attracted attention since the last century,[71] as discussed in TEXT S8. More recently, it was pointed out that the surface region of hematite particles had different compositions and structures to its interior part, which could affect the Hamaker constant.[72] Based on the data of EA and XPS analysis (Tables S2 and S8), it is reasonable to assume that UV radiation can induce changes in the dielectric properties of the DBioCs surface and cause differences between the surface and interior of the particles, thereby affecting the Hamaker constants of DBioCs. In fact, this hypothesis has been verified in other carbon materials.[43,44] Therefore, the experimentally measured attachment efficiencies (α) for pristine and photoaged DBioCs in NaCl solutions were fitted as a function of electrolyte concentrations grounded in classical DLVO theory (TEXT S9).

Good agreement between experimental data and DLVO prediction for all DBioCs ($R_{adj}^2 > 0.96$) (Figure 4a) demonstrated that their aggregation behaviors still obeyed the DLVO theory well even after UV-exposure, following the prior research.[18,63] The derived Hamaker constant for W0d in water (A_{DWD}) was $(3.19 \pm 0.11) \times 10^{-21}$ J, approaching that for PSNPs (3.5×10^{-21} J),[43] slightly smaller than those for SNPs ($7.6-7.8 \times 10^{-21}$ J)[44,73] and fullerene ($6.7-8.5 \times 10^{-21}$ J),[20,21] and much lower than those for TiO_2 (6.5×10^{-20} J)[74] and Ag NPs (13×10^{-20} J).[75] The lower A_{DWD} corresponds to a smaller van der Waals attraction between particles. Therefore, DBioCs may have colloidal stability higher than those of these widely concerned materials. Note that due to the presence of water in DBioCs voids, A_{DWD} derived here was an effective value that may be lower than the true one.[20] However, it is more relevant when assessing the DLVO interaction energies. With UV-radiation, derived Hamaker constants for DBioCs gradually decreased from 3.19 ± 0.11 (W0d) to 1.55 ± 0.07 ($\times 10^{-21}$ J) (W7d) ($p = 0.02$, Figure 4a). As depicted in eq S17, vdW energy is proportional to the Hamaker constant, A_{DWD}, and hydrodynamic radius, R. Herein, negligible discrepancy in particle sizes (Figure S6a) suggested gradually decreased vdW attraction between DBioCs. This might be the reason why W 5d and W7d required higher NaCl concentrations to reach the DLCA regime, although they were less negatively charged than W3d. It was worth mentioning that the UV-induced decrease in A_{DWD} here coincided with the result reported for PSNPs[43] but contradicted that for SNPs.[44] We believed that the photoinduced change in the Hamaker constant may depend on many factors, including particle properties, radiation conditions, etc. It warrants more systematic and comprehensive research in the future to better discern and predict the possible alteration of environmental behaviors of different particles in waters upon sunlight-exposure.

The Hamaker constant in vacuum (A_{DD}) can be approximated using the following relationship[20,62]

$$A_{DWD} = (\sqrt{A_{DD}} - \sqrt{A_{WW}})^2 \quad (1)$$

where A_{ww} is the Hamaker constant for water in vacuum, 3.7×10^{-20} J.[62] The as-obtained A_{DD} for W0d to W7d was 6.19 ± 0.05, 6.05 ± 0.03, 5.91 ± 0.04, 5.83 ± 0.03, 5.65 ± 0.06, 5.50 ± 0.05, and 5.37 ± 0.04 ($\times 10^{-20}$ J), respectively. These values fell in the range for carbon fibers ($5.2-6.2 \times 10^{-20}$ J)[71,76] and activated carbons (ACs) ($5.0-7.8 \times 10^{-20}$ J)[77] but were almost half that for NACs.[62] It indicated that there may be considerable differences in the Hamaker constant between carbon materials. The properties of different biochars may vary, depending on their feedstock, pyrolysis conditions, post-treatment, etc.[78,79] However, research on the Hamaker constant and its alterations with environmental aging for biochar colloids has rarely been studied to date. Therefore, Hamaker constants reported here are of great significance in supplementing the database of biochar characteristics.

To better understand the influence of the radiation duration on the Hamaker constant of DBioCs, A_{DWD} and A_{DD} were fitted using decay kinetic models (TEXT S10). High R_{adj}^2 (>0.94) may imply the modified first-order model and the modified second-order model can describe and predict the attenuation pattern of DBioCs' Hamaker constant well in sunlit water (Figures 4b and S14). The nondecayable components of the Hamaker constant, $A_{DWD(N)2,0}$ and $A_{DD(N)2,0}$, are 1.38×10^{-21} J and 5.26×10^{-20} J, respectively (Tables S6 and S7), and are theoretically the values that the Hamaker constants of DBioCs will eventually present under long-term photoaging. In addition, these two values can almost be converted to each other though eq 1 with the error less than 0.26%, which once again verified the accuracy of the model. The conundrum of whether the yielded values are the final A_{DWD} and A_{DD} of DBioCs that persist in real environments or they will be affected by other physicochemical processes such as adsorption or biological interactions requires further investigation. However, the models proposed here are still vital because this is the first attempt, to the best of our knowledge, to depict the changing law of Hamaker constants over time using kinetic models with very good results. Such models could be applicable in simulating where the Hamaker constant decays with time like the present work and Liu et al. study,[43] but may fail to describe those where the Hamaker constant increases with radiation like the research of Duan et al.[44] There are many reasons. On the one hand, owing to the lack of models to portray the changes in parameters, the models proposed in this study are based on the equation of chemical reaction kinetics. On the other hand, the variation in the Hamaker constant may be affected deeply by material properties and aging conditions. Accordingly, it is of great importance to dig a deeper understanding of the intrinsic relationship among materials-conditions-variations and to develop targeted models for simulating and predicting changes in environment behaviors of various particles under different aging conditions.

Furthermore, we performed Pearson correlation analysis on several important parameters (Table S9). There are significant correlations between most parameters (e.g., CCC_{Na} vs time, $r = -0.987$, $p < 0.001$) (Figure S15). A prior work argued that

https://doi.org/10.1021/acs.est.4c00780
Environ. Sci. Technol. 2024, 58, 8053−8064

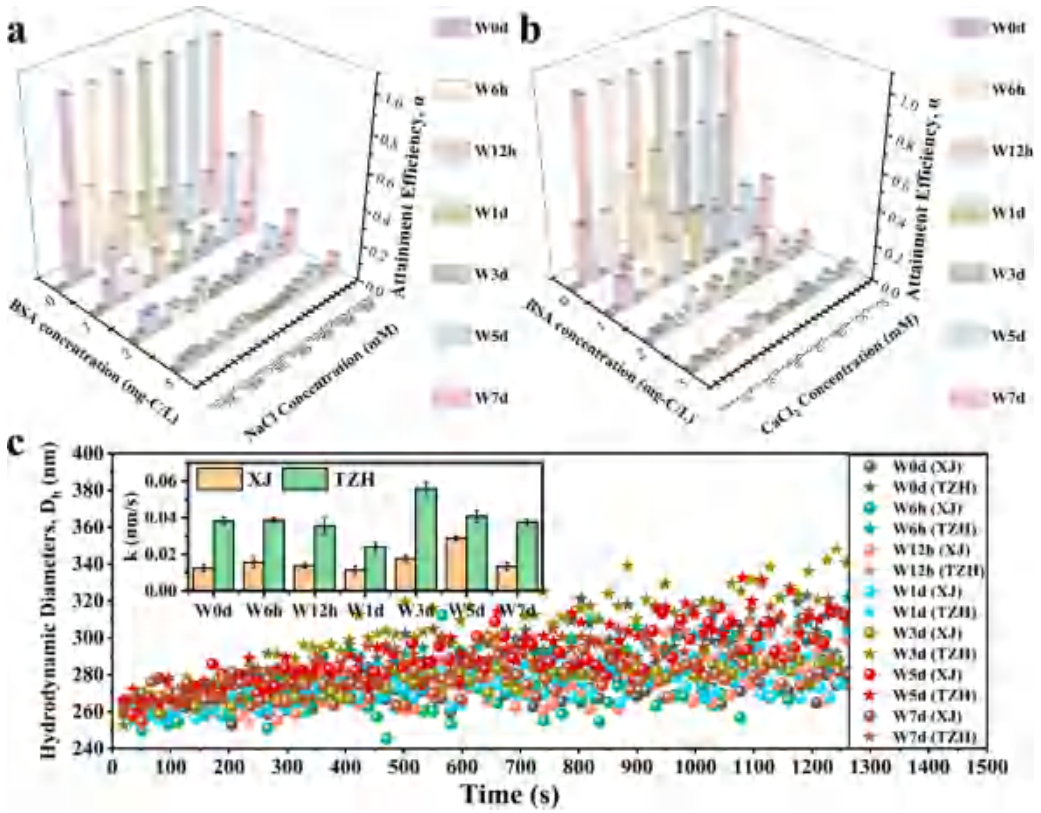

Figure 5. Aggregation behaviors of pristine and photoaged DBioCs in the presence of BSA or in the nature water samples. The variations in attachment efficiencies of DBioCs as a function of BSA concentrations (0, 1, 2, 5 mg-C/L) in (a) various NaCl (0, 10, 100, 200 mM) and (b) $CaCl_2$ concentrations (0, 1, 5, 10 mM). (c) Aggregation profiles of DBioCs in nature water samples (XJ and TZH). The inset shows the comparison of the according initial aggregation rates (k) for DBioCs before and after UV irradiation in these two water samples. All experiments were carried out at 12.5 mg-DBioCs/L and 25 °C.

CCC_{Na} significantly correlated with O/C and zeta potential.[10] Herein, the O/C ratios and CCC values were found to correlate well with radiation time ($p \leq 0.011$). However, poor correlation was observed between the ζ_0 values and radiation time ($p = 0.634$), which may signify that DBioCs experienced a multistage process during radiation.

3.5. Photoaging Mechanisms. UV-induced photooxidation of nanoparticles by ROS has been reported to result in a sustained increase in surface oxygen content and decrease in their ζ values.[43] But, UV-aged SNPs showed a monotonic decrease in surface OFGs and less negative charge due to decarboxylation.[44] Here, nonmonotonic variations in ζ_0 and CCC values over time may imply a nonsingle-factor-dominated process that DBioCs experienced under UV radiation. To deeply investigate the photoaging mechanisms, XPS spectra were thoroughly analyzed (Figures S16 and S17). The deconvolution of the C 1s peak provided three main peaks, namely underivatized carbon (C1, C-C/C-H) at 284.8 eV, mono-oxygenated carbon (C2, C-O) at ∼286.3 eV, and dioxygenated carbon (C3, C=O and O-C-O) at ∼288.5 eV,[80,81] which was assigned to sp^2 aromatic rings, epoxy and alkoxy, and carbonyl moieties, respectively.[82] The two strong O ls peaks at ∼531.5 eV and ∼533.1 eV corresponded to carbonyl and carboxyl oxygen (O1, C=O)[83] and hydroxyl and ether oxygen (O2, C-O).[84] Combining the data of FT-IR, XPS, DLS, and EA, we speculated that DBioCs could undergo three stages under UV radiation.

Stage I: W0d → W6h, featuring ζ_0 ↑, CCC_{Na} ↓, and CCC_{Ca} ↑. As known from FT-IR spectra (Figure 1c), the intensities of −OH and C−O−C peaks in W6h decreased but were opposite for the −C=C peak, relative to W0d. XPS data showed the proportions of mono/dioxygenated carbons and carbonyl oxygen reduced from 11.4%/5.8% and 27.3% to 10.7%/5.0% and 23.9%, respectively (Figure S18). Meanwhile, the bulk O/C ratio slightly decreased from 0.26 to 0.25 (Table S2). Those revealed the first 6 hours of UV radiation reduced the abundance of OFGs (−OH, −C−O, −COOH, etc.) on DBioCs surfaces, probably indicating the occurrence of photodecarboxylation.[18,38] In order to explore the variation in this stage deeply, the samples experiencing 3 and 9 hours of radiation (W3h and W9h) were prepared and meticulously characterized (Figures S19 and S20, Tables S10 and S11). From the results of FT-IR, EA, and XPS measurements, it cleared that the OFGs content of W3h is reduced compared to that of W0d, suggesting a slight decarboxylation occurred. Decarboxylation was further enhanced on W6h, but then the oxygen-bearing moieties increased on W9h. These results confirmed the DBioCs would undergo decarboxylation first when subjected to UV radiation, and it occurred mainly within 6 h. Since black carbons mainly acquire their negative charges from these OFGs,[50] the surface negative charge of DBioCs at this stage became less, and electrostatic repulsion and the CCC_{Na} value thus decreased, in line with the prior findings.[44] Furthermore, the reduced OFGs meant less binding sites to Ca^{2+} for bridging, and the CCC_{Ca} accordingly was raised.

Stage II: W6h → W3d, featuring ζ_0 ↓, CCC_{Na} ↑, and CCC_{Ca} ↓, alike to chemical aging-induced surface oxidation on DBC.[31] Under radiation, protons are absorbed and attack aromatic and

https://doi.org/10.1021/acs.est.4c00780
Environ. Sci. Technol. 2024, 58, 8053−8064

methyl moieties, producing various ROS[36,85,86] and ^{3}DBC*,[35] which may induce DBioCs surface photo-oxidation.[32] In this stage, surficial and bulk O/C and proportions of C2 and C3 continuously elevated, and the C1 proportion decreased from 84.3% to 80.4% (Figure S18a). The FT-IR peak of −C═C gradually shifted to the −C−O peak (Figure 1c). Those suggested the destruction of aromatic structures on DBioCs and the formation of OFGs. The increased OFGs not only brought more negative surface charges and stronger electrostatic repulsion, leading to higher colloidal stability of DBioCs in the NaCl solution, but also provided more bridging sites for Ca^{2+}, promoting aggregations of DBioCs in $CaCl_2$ solutions. More importantly, they may further promote the formation of ROS,[55] thus accelerating the phototransformation of DBioCs.[87] Besides, the ash content increased continuously (p = 0.003, Table S2). More exposed minerals may associate with the phenol-like structure of DBioCs, also contributing to producing ROS.[36] Given above all, the biggest dioxygenated carbon proportion and the most negative charge thus were attained after 3 days of UV-exposure.

Stage III: W3d → W7d, featuring ζ_0 ↑, CCC_{Na} ↑, and CCC_{Ca} ↓. The N element could play a vital role in producing ROS, even at low levels.[88] N content decreased steadily with radiation (p = 0.014, Table S2), implying the DBioCs surfaces were oxidized sustainedly, even after 3 days of radiation.[47] This further induced the aggregation of DBioCs in the presence of $CaCl_2$. However, ζ_0 values of W5d and W7d increased instead of decreasing (Figure S6b). The increased CCC_{Na} contradicted the weakened electrostatic repulsion, perhaps resulting from the continuous decay of the Hamaker constant, as aforementioned. The increased ζ_0 may relate to the decrease in −C═O content (Table S8). The C3 proportion fluctuated eventually between 6.1% and 6.3% (Figure S18a), probably attributed to the re-dominance of the decarboxylation effect in DBioCs with excessive carboxyl moiety. The generated ROS would attack carboxyl groups on highly oxidized COOH-MWCNTs upon UV exposure to induce decarboxylation effect.[18] Therefore, we believed that the DBioCs surface would be subjected to competition between oxidation and decarboxylation processes under UV-radiation, finally reaching dynamic equilibrium. The massive mineral exposure may be another cause for the less negative charges that DBioCs have. Most of the ash species possess more positive charges than carbon surfaces, as evidenced by the fact that the demineralized biochar has less negative zeta potential than the raw one does.[89] W5d and W7d have ash contents of 42.54% and 46.47% (Table S2). Such contents could directly affect the ζ_0 values of DBioCs.

In summary, DBioCs could suffer from multiple processes involving photodecarboxylation, photo-oxidation, and mineral-exposure under UV radiation. One of the important factors for such complex aging phenomena may be the heterogeneity of DBioCs in component, structure, and properties.[90] In real scenarios, with the complexity of the water environments, the aging process may be even more elusive.

3.6. Colloidal Stability of DBioCs in the Presence of Protein and Natural Waters. NOM has attracted wide attention due to its environmental omnipresence.[17,91,92] Figure 5a-b displayed the attachment efficiencies of DBioCs in NaCl and $CaCl_2$ solutions with the presence of BSA. Obviously, BSA can induce only a slight increase in α values in no electrolyte or very low ion concentrations (10 mM NaCl or 1 mM $CaCl_2$). It is perhaps due to the weakened surface charge caused by BSA adsorption on DBioCs (Figure S22).[93] More often, BSA significantly inhibited DBioCs aggregation, especially under IS conditions, even at very low concentrations. For instance, 1 mg-C/L of BSA can reduce the attachment efficiency of W3d from 1.00 to 0.14 at 200 mM NaCl and decline that of W1d from 1.00 to 0.32 at 10 mM $CaCl_2$. Those contradicted the less negative charges, probably attributing to the steric hindrance caused by BSA coating on the DBioCs surface, as widely reported elsewhere.[93,94] Its existence overcame the advantages arising from the reduced electrostatic repulsion and dominated the aggregation, regardless of aging degree and electrolyte type.[27] This seems to indicate that the existence of DOM in environmental water may be one of the important inducements to inhibit DBioCs aggregation.

In order to gain insight into their environmental behaviors more intuitively, the aggregation statuses of DBioCs in two natural water samples (XJ and TZH, representing river and lake waters, respectively) were investigated. As shown in Figure 5c, the aggregation rates of DBioCs in lake water were generally higher than those in the river counterpart, an expected result as the concentration of each ion in TZH was higher than that in XJ (Table S1). Correspondingly, the zeta potentials of DBioCs in TZH were less negative (Figure S23), which indicated weaker electrostatic repulsion. Nevertheless, aggregation rates of DBioCs were very low (<0.06 nm/s), even though their ζ values were higher than −30 mV. It could be related to the presence of NOM, known from TOC (2.26 mg/L for XJ and 3.65 mg/L for TZH, Table S1). As depicted before, the NOM is an important incentive to stabilize DBioCs. The higher TOC contents in the lake sample explained why the aggregation rates of DBioCs were only slightly higher in TZH despite its IS being much higher than that of XJ. In addition, as flowing water, XJ carried more suspended particles (with almost double the SS content as TZH). They had the potential to heteroaggregate with DBioCs, so as to change the colloidal stability of DBioCs.[95,96] Besides, the shear force formed by river flow could alter the aggregates structure.[97] Thereby, the fate of DBioCs in a real scenario is still fraught with much uncertainty.

Overall, the rather low aggregation rates of DBioCs in both samples indicated the environmental stability of DBioCs.[10] The discrepancy in the aggregations of pristine and aged DBioCs was not significant here (p = 0.319 for XJ and p = 0.585 for TZH). Therefore, photoaging alone may not be sufficient to dominate the aggregation of DBioCs in real waters. In fact, all environmental factors, such as water chemistries represented by salt and TOC, hydrodynamic conditions, etc., may have an impact on the behaviors of DBioCs. What role each of these factors plays in a given natural scenario requires more in-depth research.

4. ENVIRONMENTAL IMPLICATIONS

We demonstrated herein that solution chemistry, dominated by salts and TOC, exerted non-negligible impacts on the colloidal behaviors of DBC. It may reveal that DBC stably suspended in typical freshwater could experience rapid aggregation and even deposit into sediments when encountering the unexpected events areas, represented by estuaries.[98] Most of the terrestrial DBC eventually flows through rivers into the ocean, the largest sink and final home for DBC, with the amount of ∼27 Tg-C year^{-1}.[28] The DBC in deep sea was considered to possess conservative and salt-like properties but was susceptible to UV radiation.[99−101] In addition to resulting

https://doi.org/10.1021/acs.est.4c00780
Environ. Sci. Technol. 2024, 58, 8053−8064

to the loss of DBC from seawater[101] and river water,[102] sunlight can also induce DBC aging as reported in this study, thus having implications for its environmental behaviors. The decreasing Hamaker constant over time implied that the aged DBC may have higher colloidal stability. Moreover, acting as carrier, DBC can absorb contaminants or nutrients[3,9,10] and assist in their migration through freshwater, which is also largely controlled by the aggregation processes.[50] This means that in estuaries contaminants would be deposited with DBC, posing potential risks to sediment ecology. It is noteworthy that photoaging can alter the surface properties of DBC to affect its affinity and thus the amount and type of contaminants loaded.[41,86] The ROS excited from DBC under radiation can not only degrade pollutants attached it[85] but may also lead to the degradation of DBC itself thereby releasing loaded pollutants back into the water column.[103] Therefore, the environmental behavior and fate of DBC and the pollutants it carried in aquatic ecosystems can be quite complex, which deserves more attention.

The Hamaker constant derived in this study and its decay models are of particular importance for developing predictive models to quantitatively describe the fate and transport of DBC in aquatic environments. It is a long-term and arduous task to achieve this as of the extreme complexity in components of DBC and natural waters. Nevertheless, the variation in Hamaker constants induced by photoaging or other processes (e.g., chemical aging, etc.), as long as altering the surface properties, must be taken into account.

More importantly, it must be clarified that the DBioCs used in this study were prepared in the laboratory, which reflected the small fraction of DBC that is flushed out initially but omitted the larger fraction that was produced over time. It therefore may not be highly representative of fluvial DBC. Moreover, the light source used in this work has a small amount of UVC rays, and the aging is performed continuously in pure water, which ignored the potential radiation attenuation and complex interactions in actual circumstances. Thus, the variation in the Hamaker constant and the aging process of DBC in fluvial systems may be discrepant. However, the Hamaker constant and photoaging mechanisms provided in this study can serve as an important reference to comprehend the fate of DBC in sunlit waters.

■ ASSOCIATED CONTENT

Supporting Information

The Supporting Information is available free of charge at https://pubs.acs.org/doi/10.1021/acs.est.4c00780.

Details for materials preparation, radiation, characteristics, aggregation kinetics, and fitting procedures; additional discussion on pH-dependence of k_{fast} and surface-dependence of Hamaker constant, additional information about the DLVO prediction for Hamaker constants and their decay models; Figures for aging apparatus, sample sites, SEM images, DLS and zeta potential data, aggregation profiles, XPS and FT-IR spectra; Tables for water samples characteristics, elemental composition, Hamaker constants, CCC, XPS and EA data, and Pearson correlation analysis (PDF)

■ AUTHOR INFORMATION

Corresponding Author

Jie Liang − *College of Environmental Science and Engineering and Key Laboratory of Environment Biology and Pollution Control, Hunan University, Changsha 410082, P.R. China;* orcid.org/0000-0002-1979-9356; Phone: +86-731-88821413; Email: liangjie@hnu.edu.cn, liangjie82@163.com

Authors

Ning Tang − *College of Environmental Science and Engineering and Key Laboratory of Environment Biology and Pollution Control, Hunan University, Changsha 410082, P.R. China*

Yihui Guo − *College of Environmental Science and Engineering and Key Laboratory of Environment Biology and Pollution Control, Hunan University, Changsha 410082, P.R. China*

Ziqian Zhu − *College of Environmental Science and Engineering and Key Laboratory of Environment Biology and Pollution Control, Hunan University, Changsha 410082, P.R. China*

Longbo Jiang − *College of Environmental Science and Engineering and Key Laboratory of Environment Biology and Pollution Control, Hunan University, Changsha 410082, P.R. China*

Na Li − *College of Environmental Science and Engineering and Key Laboratory of Environment Biology and Pollution Control, Hunan University, Changsha 410082, P.R. China*

Tingting Hu − *College of Environmental Science and Engineering and Key Laboratory of Environment Biology and Pollution Control, Hunan University, Changsha 410082, P.R. China*

Lan Lu − *College of Environmental Science and Engineering and Key Laboratory of Environment Biology and Pollution Control, Hunan University, Changsha 410082, P.R. China*

Jingyi Zhang − *College of Environmental Science and Engineering and Key Laboratory of Environment Biology and Pollution Control, Hunan University, Changsha 410082, P.R. China*

Xiaodong Li − *College of Environmental Science and Engineering and Key Laboratory of Environment Biology and Pollution Control, Hunan University, Changsha 410082, P.R. China;* orcid.org/0000-0001-9949-7747

Complete contact information is available at: https://pubs.acs.org/10.1021/acs.est.4c00780

Notes

The authors declare no competing financial interest.

■ ACKNOWLEDGMENTS

This work was supported by the National Natural Science Foundation of China (U23A2055, 72088101, 51979101) and the Science and Technology Innovation Program of Hunan Province (2023RC1041, 2022RC1216).

■ REFERENCES

(1) Qi, Y.; Fu, W.; Tian, J.; Luo, C.; Shan, S.; Sun, S.; Ren, P.; Zhang, H.; Liu, J.; Zhang, X.; Wang, X. Dissolved black carbon is not likely a significant refractory organic carbon pool in rivers and oceans. *Nat. Commun.* **2020**, *11* (1), 5051.

(2) Coppola, A. I.; Wiedemeier, D. B.; Galy, V.; Haghipour, N.; Hanke, U. M.; Nascimento, G. S.; Usman, M.; Blattmann, T. M.; Reisser, M.; Freymond, C. V.; Zhao, M.; Voss, B.; Wacker, L.;

Schefuß, E.; Peucker-Ehrenbrink, B.; Abiven, S.; Schmidt, M. W. I.; Eglinton, T. I. Global-scale evidence for the refractory nature of riverine black carbon. *Nat. Geosci.* **2018**, *11* (8), 584−588.
(3) Lian, F.; Wang, Z. Y.; Xing, B. S. Nano-black carbon (biochar) released from pyrogenic carbonaceous matter as a super suspending agent in water/soil environments. *Biochar* **2021**, *3* (1), 1−3.
(4) Masiello, C. A.; Druffel, E. R. M. Black Carbon in Deep-sea Sediments. *Science* **1998**, *280* (5371), 1911−1913.
(5) Xiang, L.; Liu, S.; Ye, S.; Yang, H.; Song, B.; Qin, F.; Shen, M.; Tan, C.; Zeng, G.; Tan, X. Potential hazards of biochar: The negative environmental impacts of biochar applications. *J. Hazard. Mater.* **2021**, *420*, 126611.
(6) Chen, Y.; Sun, K.; Wang, Z.; Zhang, E.; Yang, Y.; Xing, B. Analytical methods, molecular structures and biogeochemical behaviors of dissolved black carbon. *Carbon Res.* **2022**, *1* (1), 23.
(7) Song, B.; Chen, M.; Zhao, L.; Qiu, H.; Cao, X. Physicochemical property and colloidal stability of micron- and nano-particle biochar derived from a variety of feedstock sources. *Sci. Total Environ.* **2019**, *661*, 685−695.
(8) Xu, Y.; Ou, Q.; Liu, C.; Zhou, X.; He, Q.; Wu, Z.; Huang, R.; Ma, J.; Lu, D.; Huangfu, X. Aggregation and deposition behaviors of dissolved black carbon with coexisting heavy metals in aquatic solution. *Environ. Sci.: Nano* **2020**, *7* (9), 2773−2784.
(9) Wang, D.; Zhang, W.; Hao, X.; Zhou, D. Transport of biochar particles in saturated granular media: effects of pyrolysis temperature and particle size. *Environ. Sci. Technol.* **2013**, *47* (2), 821−828.
(10) Liu, G.; Zheng, H.; Jiang, Z.; Zhao, J.; Wang, Z.; Pan, B.; Xing, B. Formation and Physicochemical Characteristics of Nano Biochar: Insight into Chemical and Colloidal Stability. *Environ. Sci. Technol.* **2018**, *52* (18), 10369−10379.
(11) Yang, W.; Li, B.; Shang, J. Aggregation kinetics of biochar nanoparticles in aqueous environment: Interplays of anion type and bovine serum albumin. *Sci. Total Environ.* **2022**, *833*, 155148.
(12) Trilla-Prieto, N.; Vila-Costa, M.; Casas, G.; Jiménez, B.; Dachs, J. Dissolved Black Carbon and Semivolatile Aromatic Hydrocarbons in the Ocean: Two Entangled Biogeochemical Cycles? *Environ. Sci. Technol. Lett.* **2021**, *8* (10), 918−923.
(13) Yamashita, Y.; Nakane, M.; Mori, Y.; Nishioka, J.; Ogawa, H. Fate of dissolved black carbon in the deep Pacific Ocean. *Nat. Commun.* **2022**, *13* (1), 307.
(14) Qu, X.; Fu, H.; Mao, J.; Ran, Y.; Zhang, D.; Zhu, D. Chemical and structural properties of dissolved black carbon released from biochars. *Carbon* **2016**, *96*, 759−767.
(15) Xu, F.; Wei, C.; Zeng, Q.; Li, X.; Alvarez, P. J. J.; Li, Q.; Qu, X.; Zhu, D. Aggregation Behavior of Dissolved Black Carbon: Implications for Vertical Mass Flux and Fractionation in Aquatic Systems. *Environ. Sci. Technol.* **2017**, *51* (23), 13723−13732.
(16) Chowdhury, I.; Duch, M. C.; Mansukhani, N. D.; Hersam, M. C.; Bouchard, D. Colloidal properties and stability of graphene oxide nanomaterials in the aquatic environment. *Environ. Sci. Technol.* **2013**, *47* (12), 6288−6296.
(17) Sun, B.; Zhang, Y.; Li, R.; Wang, K.; Xiao, B.; Yang, Y.; Wang, J.; Zhu, L. New insights into the colloidal stability of graphene oxide in aquatic environment: Interplays of photoaging and proteins. *Water Res.* **2021**, *200*, 117213.
(18) Hwang, Y. S.; Qu, X.; Li, Q. The role of photochemical transformations in the aggregation and deposition of carboxylated multiwall carbon nanotubes suspended in water. *Carbon* **2013**, *55*, 81−89.
(19) Qu, X.; Hwang, Y. S.; Alvarez, P. J.; Bouchard, D.; Li, Q. UV Irradiation and humic acid mediate aggregation of aqueous fullerene (nC_{60}) nanoparticles. *Environ. Sci. Technol.* **2010**, *44*, 7821−7826.
(20) Chen, K. L.; Elimelech, M. Aggregation and Deposition Kinetics of Fullerene (C_{60}) Nanoparticles. *Langmuir* **2006**, *22*, 10994−11001.
(21) Chen, K. L.; Elimelech, M. Relating colloidal stability of fullerene (C_{60}) nanoparticles to nanoparticle charge and electrokinetic properties. *Environ. Sci. Technol.* **2009**, *43*, 7270−7276.
(22) Wang, H.; Dong, Y.; Zhu, M.; Li, X.; Keller, A. A.; Wang, T.; Li, F. Heteroaggregation of engineered nanoparticles and kaolin clays in aqueous environments. *Water Res.* **2015**, *80*, 130−138.
(23) Fernando, I.; Lu, D.; Zhou, Y. Interactive influence of extracellular polymeric substances (EPS) and electrolytes on the colloidal stability of silver nanoparticles. *Environ. Sci.: Nano* **2020**, *7* (1), 186−197.
(24) Tiwari, E.; Khandelwal, N.; Singh, N.; Biswas, S.; Darbha, G. K. Effect of clay colloid - CuO nanoparticles interaction on retention of nanoparticles in different types of soils: role of clay fraction and environmental parameters. *Environ. Res.* **2022**, *203*, 111885.
(25) Li, X.; He, E.; Zhang, M.; Peijnenburg, W.; Liu, Y.; Song, L.; Cao, X.; Zhao, L.; Qiu, H. Interactions of CeO_2 nanoparticles with natural colloids and electrolytes impact their aggregation kinetics and colloidal stability. *J. Hazard. Mater.* **2020**, *386*, 121973.
(26) Li, X.; Ji, S.; He, E.; Peijnenburg, W.; Cao, X.; Zhao, L.; Xu, X.; Zhang, P.; Qiu, H. UV/ozone induced physicochemical transformations of polystyrene nanoparticles and their aggregation tendency and kinetics with natural organic matter in aqueous systems. *J. Hazard. Mater.* **2022**, *433*, 128790.
(27) Liu, Y.; Huang, Z.; Zhou, J.; Tang, J.; Yang, C.; Chen, C.; Huang, W.; Dang, Z. Influence of environmental and biological macromolecules on aggregation kinetics of nanoplastics in aquatic systems. *Water Res.* **2020**, *186*, 116316.
(28) Jaffé, R.; DING, Y.; Niggemann, J.; Vähätalo, A. V.; Stubbins, A.; Spencer, R. G. M.; Campbell, J.; Dittmar, T. Global Charcoal Mobilization from Soils via Dissolution and Riverine Transport to the Oceans. *Science* **2013**, *340*, 345−347.
(29) Yang, K.; Wang, X.; Cheng, H.; Tao, S. Effect of aging on stabilization of Cd and Ni by biochars and enzyme activities in a historically contaminated alkaline agricultural soil simulated with wet-dry and freeze-thaw cycling. *Environ. Pollut.* **2021**, *268*, 115846.
(30) Meng, Z.; Huang, S.; Xu, T.; Deng, Y.; Lin, Z.; Wang, X. Transport and transformation of Cd between biochar and soil under combined dry-wet and freeze-thaw aging. *Environ. Pollut.* **2020**, *263*, 114449.
(31) Wang, Y.; Zhang, W.; Shang, J.; Shen, C.; Joseph, S. D. Chemical Aging Changed Aggregation Kinetics and Transport of Biochar Colloids. *Environ. Sci. Technol.* **2019**, *53* (14), 8136−8146.
(32) Wang, L.; O'Connor, D.; Rinklebe, J.; Ok, Y. S.; Tsang, D. C. W.; Shen, Z.; Hou, D. Biochar Aging: Mechanisms, Physicochemical Changes, Assessment, And Implications for Field Applications. *Environ. Sci. Technol.* **2020**, *54* (23), 14797−14814.
(33) Nidheesh, P. V.; Gopinath, A.; Ranjith, N.; Praveen, A. A.; Sreedharan, V.; Suresh, K. M. Potential role of biochar in advanced oxidation processes: A sustainable approach. *Chem. Eng. J.* **2021**, *405*, 126582.
(34) Wan, D.; Wang, J.; Dionysiou, D. D.; Kong, Y.; Yao, W.; Selvinsimpson, S.; Chen, Y. Photogeneration of Reactive Species from Biochar-Derived Dissolved Black Carbon for the Degradation of Amine and Phenolic Pollutants. *Environ. Sci. Technol.* **2021**, *55* (13), 8866−8876.
(35) Shi, H.; Wang, M.; Wang, B.; Huang, Q.; Gao, S. Insights on photochemical activities of organic components and minerals in dissolved state biochar in the degradation of atorvastatin in aqueous solution. *J. Hazard. Mater.* **2020**, *392*, 122277.
(36) Fu, H.; Liu, H.; Mao, J.; Chu, W.; Li, Q.; Alvarez, P. J.; Qu, X.; Zhu, D. Photochemistry of Dissolved Black Carbon Released from Biochar: Reactive Oxygen Species Generation and Phototransformation. *Environ. Sci. Technol.* **2016**, *50* (3), 1218−1226.
(37) Ward, C. P.; Sleighter, R. L.; Hatcher, P. G.; Cory, R. M. Insights into the complete and partial photooxidation of black carbon in surface waters. *Environ. Sci.: Process Impacts* **2014**, *16* (4), 721−731.
(38) Liu, Y.; Wang, M.; Yin, S.; Xie, L.; Qu, X.; Fu, H.; Shi, Q.; Zhou, F.; Xu, F.; Tao, S.; Zhu, D. Comparing Photoactivities of Dissolved Organic Matter Released from Rice Straw-Pyrolyzed Biochar and Composted Rice Straw. *Environ. Sci. Technol.* **2022**, *56* (4), 2803−2815.

https://doi.org/10.1021/acs.est.4c00780
Environ. Sci. Technol. 2024, 58, 8053−8064

(39) Wang, H.; Zhou, H.; Ma, J.; Nie, J.; Yan, S.; Song, W. Triplet Photochemistry of Dissolved Black Carbon and Its Effects on the Photochemical Formation of Reactive Oxygen Species. *Environ. Sci. Technol.* **2020**, *54* (8), 4903−4911.
(40) Fang, J.; Cheng, L.; Hameed, R.; Jin, L.; Wang, D.; Owens, G.; Lin, D. Release and stability of water dispersible biochar colloids in aquatic environments: Effects of pyrolysis temperature, particle size, and solution chemistry. *Environ. Pollut.* **2020**, *260*, 114037.
(41) Lian, F.; Zhang, Y.; Gu, S.; Han, Y.; Cao, X.; Wang, Z.; Xing, B. Photochemical Transformation and Catalytic Activity of Dissolved Black Nitrogen Released from Environmental Black Carbon. *Environ. Sci. Technol.* **2021**, *55* (9), 6476−6484.
(42) Fronczak, S. G.; Dong, J.; Browne, C. A.; Krenek, E. C.; Franses, E. I.; Beaudoin, S. P.; Corti, D. S. A New "Quasi-Dynamic" Method for Determining the Hamaker Constant of Solids Using an Atomic Force Microscope. *Langmuir* **2017**, *33* (3), 714−725.
(43) Liu, Y.; Hu, Y.; Yang, C.; Chen, C.; Huang, W.; Dang, Z. Aggregation kinetics of UV irradiated nanoplastics in aquatic environments. *Water Res.* **2019**, *163*, 114870.
(44) Duan, Z.; Wang, P.; Yu, G.; Liang, M.; Dong, J.; Su, J.; Huang, W.; Li, Y.; Zhang, A.; Chen, C. Aggregation kinetics of UV-aged soot nanoparticles in wet environments: Effects of irradiation time and background solution chemistry. *Water Res.* **2021**, *201*, 117385.
(45) Zhu, K.; Jia, H.; Sun, Y.; Dai, Y.; Zhang, C.; Guo, X.; Wang, T.; Zhu, L. Long-term phototransformation of microplastics under simulated sunlight irradiation in aquatic environments: Roles of reactive oxygen species. *Water Res.* **2020**, *173*, 115564.
(46) Zhu, Z.; Li, X.; Bu, Q.; Yan, Q.; Wen, L.; Chen, X.; Li, X.; Yan, M.; Jiang, L.; Chen, G.; Li, S.; Gao, X.; Zeng, G.; Liang, J. Land−Water Transport and Sources of Nitrogen Pollution Affecting the Structure and Function of Riverine Microbial Communities. *Environ. Sci. Technol.* **2023**, *57*, 2726−2738.
(47) Li, N.; Rao, F.; He, L.; Yang, S.; Bao, Y.; Huang, C.; Bao, M.; Chen, Y. Evaluation of biochar properties exposing to solar radiation: A promotion on surface activities. *Chem. Eng. J.* **2020**, *384*, 123353.
(48) Aller, M. F. Biochar properties: Transport, fate, and impact. *Crit. Rev. Environ. Sci. Technol.* **2016**, *46* (14−15), 1183−1296.
(49) Singh, N.; Bhagat, J.; Tiwari, E.; Khandelwal, N.; Darbha, G. K.; Shyama, S. K. Metal oxide nanoparticles and polycyclic aromatic hydrocarbons alter nanoplastic's stability and toxicity to zebrafish. *J. Hazard. Mater.* **2021**, *407*, 124382.
(50) Chen, C.; Huang, W. Aggregation Kinetics of Diesel Soot Nanoparticles in Wet Environments. *Environ. Sci. Technol.* **2017**, *51* (4), 2077−2086.
(51) Lian, F.; Yu, W.; Wang, Z.; Xing, B. New Insights into Black Carbon Nanoparticle-Induced Dispersibility of Goethite Colloids and Configuration-Dependent Sorption for Phenanthrene. *Environ. Sci. Technol.* **2019**, *53* (2), 661−670.
(52) Tang, N.; Niu, C. G.; Li, X. T.; Liang, C.; Guo, H.; Lin, L. S.; Zheng, C.; Zeng, G. Efficient removal of Cd^{2+} and Pb^{2+} from aqueous solution with amino- and thiol-functionalized activated carbon: Isotherm and kinetics modeling. *Sci. Total Environ.* **2018**, *635*, 1331−1344.
(53) Wang, B.; Shang, C.; Xie, H.; Sun, H.; Zhang, Q.; Xue, L.; Tack, F. M. G.; Hou, D.; Feng, Y.; Rinklebe, J. Unraveling natural aging-induced properties change of sludge-derived hydrochar and enhanced cadmium sorption site heterogeneity. *Biochar* **2022**, *4* (1), 34.
(54) Alam, M. S.; Gorman-Lewis, D.; Chen, N.; Flynn, S. L.; Ok, Y. S.; Konhauser, K. O.; Alessi, D. S. Thermodynamic Analysis of Nickel(II) and Zinc(II) Adsorption to Biochar. *Environ. Sci. Technol.* **2018**, *52* (11), 6246−6255.
(55) Chen, N.; Huang, Y.; Hou, X.; Ai, Z.; Zhang, L. Photochemistry of Hydrochar: Reactive Oxygen Species Generation and Sulfadimidine Degradation. *Environ. Sci. Technol.* **2017**, *51* (19), 11278−11287.
(56) Li, X.; He, E.; Xia, B.; Van Gestel, C. A. M.; Peijnenburg, W.; Cao, X.; Qiu, H. Impact of CeO_2 nanoparticles on the aggregation kinetics and stability of polystyrene nanoplastics: Importance of surface functionalization and solution chemistry. *Water Res.* **2020**, *186*, 116324.
(57) Mohona, T. M.; Gupta, A.; Masud, A.; Chien, S. C.; Lin, L. C.; Nalam, P. C.; Aich, N. Aggregation Behavior of Inorganic 2D Nanomaterials Beyond Graphene: Insights from Molecular Modeling and Modified DLVO Theory. *Environ. Sci. Technol.* **2019**, *53* (8), 4161−4172.
(58) Shao, Z.; Luo, S.; Liang, M.; Ning, Z.; Sun, W.; Zhu, Y.; Mo, J.; Li, Y.; Huang, W.; Chen, C. Colloidal stability of nanosized activated carbon in aquatic systems: Effects of pH, electrolytes, and macromolecules. *Water Res.* **2021**, *203*, 117561.
(59) Smith, B.; Wepasnick, K.; Schrote, K. E.; Bertele, A. R.; Ball, W. P.; O'Melia, C.; Fairbrother, H. Colloidal properties of aqueous suspensions of acid-treated, multi-walled carbon nanotubes. *Environ. Sci. Technol.* **2009**, *43*, 819−825.
(60) Tang, H.; Zhao, Y.; Yang, X.; Liu, D.; Shao, P.; Zhu, Z.; Shan, S.; Cui, F.; Xing, B. New Insight into the Aggregation of Graphene Oxide Using Molecular Dynamics Simulations and Extended Derjaguin-Landau-Verwey-Overbeek Theory. *Environ. Sci. Technol.* **2017**, *51* (17), 9674−9682.
(61) Guo, Y.; Tang, N.; Guo, J.; Lu, L.; Li, N.; Hu, T.; Zhu, Z.; Gao, X.; Li, X.; Jiang, L.; Liang, J. The aggregation of natural inorganic colloids in aqueous environment: A review. *Chemosphere* **2023**, *310*, 136805.
(62) Chen, C.; Huang, W. Aggregation kinetics of nanosized activated carbons in aquatic environments. *Chem. Eng. J.* **2017**, *313*, 882−889.
(63) Zhang, H.; Sun, J.; Guo, L.-H. UV irradiation mediated aggregation of TiO_2 nanoparticles in simulated aquatic system. *NanoImpact* **2016**, *3*−*4*, 75−80.
(64) Tan, Z.; Yin, Y.; Guo, X.; Wang, B.; Shang, H.; Xu, J.; Zhao, Q.; Liu, J.; Xing, B. Natural organic matter inhibits aggregation of few-layered black phosphorus in mono- and divalent electrolyte solutions. *Environ. Sci.: Nano* **2019**, *6* (2), 599−609.
(65) Yang, W.; Shang, J.; Sharma, P.; Li, B.; Liu, K.; Flury, M. Colloidal stability and aggregation kinetics of biochar colloids: Effects of pyrolysis temperature, cation type, and humic acid concentrations. *Sci. Total Environ.* **2019**, *658*, 1306−1315.
(66) Deline, A. R.; Frank, B. P.; Smith, C. L.; Sigmon, L. R.; Wallace, A. N.; Gallagher, M. J.; Goodwin, D. G., Jr.; Durkin, D. P.; Fairbrother, D. H. Influence of Oxygen-Containing Functional Groups on the Environmental Properties, Transformations, and Toxicity of Carbon Nanotubes. *Chem. Rev.* **2020**, *120* (20), 11651−11697.
(67) Yang, K.; Chen, B.; Zhu, X.; Xing, B. Aggregation, Adsorption, and Morphological Transformation of Graphene Oxide in Aqueous Solutions Containing Different Metal Cations. *Environ. Sci. Technol.* **2016**, *50* (20), 11066−11075.
(68) Kim, C.; Fortner, J. D. Surface-Engineered Nanomaterials in Water: Understanding Critical Dynamics of Soft Organic Coatings and Relative Aggregation Density. *Environ. Sci. Technol.* **2020**, *54* (21), 13548−13555.
(69) Parsegian, V. A. *Van der Waals Forces: A Handbook for Biologists, Chemists, Engineers, and Physicists*. Cambridge University Press: New York, 2006.
(70) Capco, D. G.; Chen, Y. *Nanomaterial Impacts on Cell Biology and Medicine*. Springer Dordrecht Heidelberg: New York London, 2014; pp 24−43.
(71) Morra, M.; Occhiello, E.; Garbassi, F. Effect of surface treatment on the Hamaker constant of intermediate modulus carbon fibers. *Colloid Polym. Sci.* **1992**, *270* (1), 58−63.
(72) Sayano, A.; Shinozaki, K.; Ohshima, H.; Yasuda, K.; Tsurumi, T. Variations in the Hamaker constant of hematite particles in water. *Colloids Surf., A* **2022**, *654*, 129368.
(73) Li, J.; Yang, X.; Zhang, Z.; Xiao, H.; Sun, W.; Huang, W.; Li, Y.; Chen, C.; Sun, Y. Aggregation kinetics of diesel soot nanoparticles in artificial and human sweat solutions: Effects of sweat constituents, pH, and temperature. *J. Hazard. Mater.* **2021**, *403*, 123614.

https://doi.org/10.1021/acs.est.4c00780
Environ. Sci. Technol. 2024, 58, 8053−8064

(74) Liu, X.; Chen, G.; Su, C. Effects of material properties on sedimentation and aggregation of titanium dioxide nanoparticles of anatase and rutile in the aqueous phase. *J. Colloid Interface Sci.* **2011**, *363* (1), 84−91.
(75) Zhou, D.; Abdel-Fattah, A. I.; Keller, A. A. Clay particles destabilize engineered nanoparticles in aqueous environments. *Environ. Sci. Technol.* **2012**, *46* (14), 7520−7526.
(76) Maurer, S.; Mersmann, A.; Peukert, W. Henry coefficients of adsorption predicted from solid Hamaker constants. *Chem. Eng. Sci.* **2001**, *56*, 3443−3453.
(77) Peukert, W.; Mehler, C.; Götzinger, M. Novel concepts for characterisation of heterogeneous particulate surfaces. *Appl. Surf. Sci.* **2002**, *196*, 30−40.
(78) Liu, W.; Jiang, H.; Yu, H. Development of Biochar-Based Functional Materials: Toward a Sustainable Platform Carbon Material. *Chem. Rev.* **2015**, *115* (22), 12251−12285.
(79) Lian, F.; Xing, B. S. Black Carbon (Biochar) In Water/Soil Environments: Molecular Structure, Sorption, Stability, and Potential Risk. *Environ. Sci. Technol.* **2017**, *51* (23), 13517−13532.
(80) Lee, J.; Cho, M.; Fortner, J. D.; Hughes, J. B.; Kim, J.-H. Transformation of aggregated C_{60} in the aqueous phase by UV irradiation. *Environ. Sci. Technol.* **2009**, *43*, 4878−4883.
(81) Xing, W.; Luo, K.; Liang, J.; Su, C.; Tang, W. Urchin-like core−shell tungsten oxide@carbon composite electrode for highly efficient and stable water desalination via hybrid capacitive deionization (HCDI). *Chem. Eng. J.* **2023**, *477*, 147268.
(82) Ma, J.; Sun, Y.; Zhang, M.; Yang, M.; Gong, X.; Yu, F.; Zheng, J. Comparative Study of Graphene Hydrogels and Aerogels Reveals the Important Role of Buried Water in Pollutant Adsorption. *Environ. Sci. Technol.* **2017**, *51* (21), 12283−12292.
(83) Wang, D.; Jin, Y.; Park, C. M.; Heo, J.; Bai, X.; Aich, N.; Su, C. Modeling the Transport of the "New-Horizon" Reduced Graphene Oxide-Metal Oxide Nanohybrids in Water-Saturated Porous Media. *Environ. Sci. Technol.* **2018**, *52* (8), 4610−4622.
(84) Qian, X.; Ren, M.; Zhu, Y.; Yue, D.; Han, Y.; Jia, J.; Zhao, Y. Visible Light Assisted Heterogeneous Fenton-Like Degradation of Organic Pollutant via α-FeOOH/Mesoporous Carbon Composites. *Environ. Sci. Technol.* **2017**, *51* (7), 3993−4000.
(85) Fang, G.; Liu, C.; Wang, Y.; Dionysiou, D. D.; Zhou, D. Photogeneration of reactive oxygen species from biochar suspension for diethyl phthalate degradation. *Appl. Catal., B* **2017**, *214*, 34−45.
(86) Li, L.; Wang, X.; Fu, H.; Qu, X.; Chen, J.; Tao, S.; Zhu, D. Dissolved Black Carbon Facilitates Photoreduction of Hg(II) to Hg(0) and Reduces Mercury Uptake by Lettuce (Lactuca sativa L.). *Environ. Sci. Technol.* **2020**, *54* (18), 11137−11145.
(87) Xiao, Y.; Lyu, H.; Tang, J.; Wang, K.; Sun, H. Effects of ball milling on the photochemistry of biochar: Enrofloxacin degradation and possible mechanisms. *Chem. Eng. J.* **2020**, *384*, 123311.
(88) Yang, J.; Zhu, W.; Yao, Q.; Lu, G.; Yang, C.; Dang, Z. Photochemical reactivity of nitrogen-doped biochars under simulated sunlight irradiation: Generation of singlet oxygen. *J. Hazard. Mater.* **2021**, *410*, 124547.
(89) Tao, S.; Liang, S.; Chen, Y.; Yu, W.; Hou, H.; Qiu, J.; Zhu, Y.; Xiao, K.; Hu, J.; Liu, B.; Wang, Y.; Yang, J. Enhanced sludge dewaterability with sludge-derived biochar activating hydrogen peroxide: Synergism of Fe and Al elements in biochar. *Water Res.* **2020**, *182*, 115927.
(90) Zhao, L.; Cao, X.; Masek, O.; Zimmerman, A. Heterogeneity of biochar properties as a function of feedstock sources and production temperatures. *J. Hazard. Mater.* **2013**, *256*−*257*, 1−9.
(91) Sun, B.; Zhang, Y.; Chen, W.; Wang, K.; Zhu, L. Concentration Dependent Effects of Bovine Serum Albumin on Graphene Oxide Colloidal Stability in Aquatic Environment. *Environ. Sci. Technol.* **2018**, *52* (13), 7212−7219.
(92) Zhang, M.; Shen, X.; Zhang, H.; Werner, D.; Wang, B.; Yang, Y.; Tao, S.; Wang, X. Humic Acid Can Enhance the Mineralization of Phenanthrene Sorbed on Biochars. *Environ. Sci. Technol.* **2019**, *53* (22), 13201−13208.
(93) Guo, Y.; Tang, N.; Lu, L.; Li, N.; Hu, T.; Guo, J.; Zhang, J.; Zeng, Z.; Liang, J. Aggregation behavior of polystyrene nanoplastics: Role of surface functional groups and protein and electrolyte variation. *Chemosphere* **2024**, *350*, 140998.
(94) Ren, M.; Horn, H.; Frimmel, F. H. Aggregation behavior of TiO_2 nanoparticles in municipal effluent: Influence of ionic strengthen and organic compounds. *Water Res.* **2017**, *123*, 678−686.
(95) Gui, X.; Song, B.; Chen, M.; Xu, X.; Ren, Z.; Li, X.; Cao, X. Soil colloids affect the aggregation and stability of biochar colloids. *Sci. Total Environ.* **2021**, *771*, 145414.
(96) Liu, Y.; Ma, J.; Gao, J.; Chen, X.; Ouyang, X.; Weng, L.; Li, H.; Chen, Y.; Li, Y. Stability and interaction of biochar and iron mineral nanoparticles: effect of pH, ionic strength, and dissolved organic matter. *Biochar* **2022**, *4* (1), 47.
(97) Frungieri, G.; Babler, M. U.; Vanni, M. Shear-Induced Heteroaggregation of Oppositely Charged Colloidal Particles. *Langmuir* **2020**, *36* (36), 10739−10749.
(98) Marques, J. S. J.; Dittmar, T.; Niggemann, J.; Almeida, M. G.; Gomez-Saez, G. V.; Rezende, C. E. Dissolved Black Carbon in the Headwaters-to-Ocean Continuum of Paraiba Do Sul River. *Brazil. Front. Earth Sci.* **2017**, *5*, 11.
(99) Dittmar, T.; Paeng, J. A heat-induced molecular signature in marine dissolved organic matter. *Nat. Geosci.* **2009**, *2* (3), 175−179.
(100) Ziolkowski, L. A.; Druffel, E. R. M. Aged black carbon identified in marine dissolved organic carbon. *Geophys. Res. Lett.* **2010**, *37*, L16601.
(101) Stubbins, A.; Niggemann, J.; Dittmar, T. Photo-lability of deep ocean dissolved black carbon. *Biogeosciences* **2012**, *9* (5), 1661−1670.
(102) Riedel, T.; Zark, M.; Vahatalo, A. V.; Niggemann, J.; Spencer, R. G. M.; Hernes, P. J.; Dittmar, T. Molecular Signatures of Biogeochemical Transformations in Dissolved Organic Matter from Ten World Rivers. *Front. Earth Sci.* **2016**, *4*, 85.
(103) Zhang, R.; Deng, Z.; Li, J.; Zhang, Y.; Wei, Z.; Cao, H. Effect of leaching time on phytotoxicity of dissolved organic matter derived from black carbon based on spectroscopy. *Environ. Pollut.* **2022**, *307*, 119595.

NOTE ADDED AFTER ASAP PUBLICATION

Due to a production error, the version of this paper that was published ASAP April 25, 2024, had a typo in the title. The corrected version was reposted May 7, 2024.

https://doi.org/10.1021/acs.est.4c00780
Environ. Sci. Technol. 2024, 58, 8053−8064